

# Convergence of Ray- and Pixel-Driven Discretization Frameworks in the Strong Operator Topology

Richard Huber<sup>1</sup>[0000-0003-1743-6786]

Technical University of Denmark  
Department of Applied Mathematics and Computer Science  
2800 Kgs. Lyngby, Denmark  
richu@dtu.dk

**Abstract.** Tomography is a central tool in medical applications, allowing doctors to investigate patients' interior features. The Radon transform is commonly used to model the corresponding measurement process. Since in any practical application one can only obtain and process finitely many measurements, suitable discretization of the Radon transform and its adjoint (called the backprojection) is crucial. The most commonly used discretization approach combines the ray-driven Radon transform with the pixel-driven backprojection, as anecdotal reports describe these as showing the best approximation performance. However, there is little rigorous understanding of induced approximation errors. These methods involve three discretization parameters: the spatial-, detector-, and angular resolutions. Most commonly, balanced resolutions are used, i.e., the same (or similar) spatial- and detector resolutions. We present a novel interpretation of ray- and pixel-driven discretizations as 'convolutional methods'. This allows for a structured analysis that can explain observed behavior. In particular, we prove convergence in the strong operator topology of the ray-driven Radon transform and the pixel-driven backprojection under suitable choice of discretization parameters. Notably, said suitable parameter choices include the combination of the ray-driven Radon transform with the pixel-driven backprojection under balanced resolutions, thus theoretically justifying this approach. Our theoretical investigations are complemented by numerical experiments that show behavior in simulations that the theory predicted or suggested. **These numerical simulations are still missing from this version of the paper!**

**Keywords:** Radon Transform · Computed Tomography · Discretization Errors · Numerical Analysis · X-ray Transform.

## 1 Introduction

Computed Tomography (CT) is a crucial tool in medicine, allowing the investigation of the interior of patients' bodies [8]. The measurement process consists of observing the intensity of radiation that traveled through the patient after

being emitted on the opposite side. Said radiation is assumed to move along straight lines through the patient and loses intensity due to attenuation when transversing matter; thus the loss of intensity is related to the transversed density of the body. In the parallel beam case, this process is commonly modeled by the Radon transform  $\mathcal{R}$  [3,14] (in this context also forward operator) that maps a function  $f$  describing the mass-density distribution in the body onto a function  $\mathcal{R}f$  describing measurements along all measured straight lines (parametrized by an angular variable  $\phi$  and a detector variable  $s$ ). Hence, this transform is a line integral operator representing the accumulation of attenuation along straight lines. Therefore, the (parallel-beam) tomographic reconstruction corresponds to the solution of the inverse problem  $\mathcal{R}f = g$  for known measurements  $g$  and unknown density distributions  $f$ .

While there is a direct inversion formula called the filtered backprojection [14], many more evolved reconstruction techniques are iterative, e.g., iterative algebraic reconstruction algorithms [7,1,17] and solution algorithms for convex optimization problems (e.g., total variation regularized reconstructions) [18,4,11]. These iterative methods also involve the adjoint operator  $\mathcal{R}^*$  (called the backprojection [14]).

Only finite amounts of data can be measured and processed for practical applications. Thus, proper discretization  $\mathcal{R}_\delta$  (for some discretization parameters  $\delta$ ) is imperative. It is common to think of both measurements and reconstructions as images with pixels of finite resolutions and correspondingly,  $\delta = (\delta_x, \delta_\phi, \delta_s)$  denotes the spatial resolution of reconstructions  $\delta_x$ , and the angular- and detector resolutions  $(\delta_\phi, \delta_s)$  of measured data. The expectation is that with ever finer resolution ( $\delta \rightarrow 0$ ), also the approximation gets better (i.e.,  $\mathcal{R}_\delta \xrightarrow{\delta \rightarrow 0} \mathcal{R}$  in some sense). Simultaneously, the approximations of the backprojection should also improve with higher degrees of discretization. This is crucial, as it justifies the use of theory concerning the (continuous) Radon transform to discrete settings.

The most widely used discretization framework uses the ray-driven Radon transform  $\mathcal{R}_\delta^{\text{rd}}$  [19,20,6] and the pixel-driven backprojection  $\mathcal{R}_\delta^{\text{pd}^*}$  [15,21,16,2] (we speak of an rd-pd\* approach). Concerning the choice of discretization parameters  $\delta$ , it is most common to use balanced resolutions, i.e.,  $\delta_x \approx \delta_s$ . Note that usually  $\delta_\phi$  and  $\delta_s$  are determined from the measurements, while  $\delta_x$  is somewhat electable. The ray-driven approach discretizes line integrals by summation of integrals on line intersections with pixels, while the pixel-driven backprojection is based on linear interpolation on the detector. There is also a ray-driven backprojection and a pixel-driven Radon transform as the adjoints to the mentioned operators, however, these are said to perform poorly (supposedly creating artifacts [12]) and are thus hardly ever used in practice.

Not using the forward and backprojections from the same framework (i.e., rd-pd\* rather than rd-rd\* or pd-pd\*) can potentially harm iterative solvers [5,13]. The reason is that convergence guarantees of many iterative solvers (or iterative optimization algorithms, more generally) are based on adjointness yielding some orthogonality properties. Thus, such methods might converge more slowly or not fully converge when using non-adjoint (unmatched) operator pairs.

However, this danger seems to be outweighed in practice by the supposed better approximation performance of the rd-pd\* methods. Using mismatched operators is certainly preferable to discretizations that do not properly represent the measurement process. There is little rigorous analysis of approximation errors, and anecdotal knowledge of performance is much more prevalent. In [2], the author rigorously discussed approximation errors for pixel-driven methods in the case the spatial resolution  $\delta_x$  is asymptotically smaller than the detector resolution  $\delta_s$ , finding convergence in the operator norm, thus justifying the pd-pd\* approach when  $\frac{\delta_x}{\delta_s} \rightarrow 0$ . However, in practice, it is much more common to use balanced resolutions ( $\delta_x \approx \delta_s$ ), in which case these results are not applicable.

This paper will justify the use of rd-pd\* approaches for balanced resolutions by proving convergence in the strong operator topology (i.e., pointwise convergence). This substantiates heuristic notions of approximation performance. In particular, given any function, the resolutions can be chosen fine enough to approximate the Radon transform (or backprojection) arbitrarily well. Some of these results were already presented in the author’s doctoral thesis [9]. Moreover, we show that convergence of the ray-driven backprojection is obtained if  $\delta_s \ll \delta_x$ . The main theoretical result Theorem 1 was already announced in [10] without a rigorous proof, which this paper now provides.

This paper is structured as follows: Section 2 describes the Radon transform and related notation (Section 2.1) and the investigated discretization frameworks (Section 2.2). We perform a convergence analysis to investigate the approximation properties of these discretizations in Section 3, resulting in the main theoretical result in Theorem 1. Finally, Section 4 presents numerical experiments corroborating these theoretical results.

## 2 The Discrete Radon Transform

Below, we set the notation, give relevant definitions, as well as introduce the considered discretization frameworks.

### 2.1 Preliminaries and notation

Throughout this paper, we denote the spatial domain by  $\Omega := B(0, 1) \subset \mathbb{R}^2$ ; one can think of it as the area in which the investigated body is located. All investigations in this paper will be planar, i.e., we ignore the natural third space dimension. This domain is complemented by the sinogram domain representing all measurement points.

**Definition 1 (Sinogram domain).** *We define the (parallel-beam) sinogram domain  $\mathcal{S} := [0, \pi[\times] - 1, 1[$ . Moreover, given  $(\phi, s) \in \mathcal{S}$ , the associated straight line is  $L_{\phi,s} := \{s\vartheta_\phi + t\vartheta_\phi^\perp \in \mathbb{R}^2 \mid t \in \mathbb{R}\}$ , where  $\vartheta_\phi := (\cos(\phi), \sin(\phi)) \in \mathbb{R}^2$  is the unit vector associated with the angle  $\phi$  and  $\vartheta_\phi^\perp := (-\sin(\phi), \cos(\phi)) \in \mathbb{R}^2$  denotes the direction rotated by 90 degrees counterclockwise; see Figure 1.*

*Remark 1.* Note that other choices for the angular domain concerning  $\phi$  are possible, e.g.,  $[-\frac{\pi}{2}, \frac{\pi}{2}[$ , or  $[0, 2\pi[$ , and are also used throughout the literature. Due to the symmetry properties of the Radon transform, these formulations are equivalent as long as the angular domain's  $\pi$ -periodic projection fills  $[0, \pi[$ .

The (theoretical) measurement process can be understood as granting one measurement value for each  $(\phi, s) \in \mathcal{S}$  related to line integrals along  $L_{\phi, s}$ , resulting in the Radon transform.

**Definition 2 (Radon transform).** *The Radon transform  $\mathcal{R}: L^2(\Omega) \rightarrow L^2(\mathcal{S})$  is defined according to*

$$[\mathcal{R}f](\phi, s) := \int_{\mathbb{R}^2} f(x) \, d\mathcal{H}^1 \llcorner L_{\phi, s}(x) = \int_{\mathbb{R}} f(s\vartheta_\phi + t\vartheta_\phi^\perp) \, dt \quad (1)$$

for  $f \in L^2(\Omega)$  and  $(\phi, s) \in \mathcal{S}$  (where  $\mathcal{H}^1 \llcorner L_{\phi, s}$  denotes the one-dimensional Hausdorff measure restricted to  $L_{\phi, s}$ ), i.e., a collection of line integrals.

We define the (parallel-beam) backprojection  $\mathcal{R}^*: L^2(\mathcal{S}) \rightarrow L^2(\Omega)$ , which, given  $g \in L^2(\mathcal{S})$ , reads

$$[\mathcal{R}^*g](x) := \int_0^\pi g(\phi, x \cdot \vartheta_\phi) \, d\phi \quad \text{for } x \in \Omega. \quad (2)$$

As is common,  $L^2(\Omega)$  denotes the set of functions (or rather equivalence classes of Lebesgue almost everywhere equal functions)  $f: \Omega \rightarrow \mathbb{R}$  such that  $\|f\|_{L^2(\Omega)}^2 := \int_\Omega |f(x)|^2 \, dx < \infty$ , and analogously for  $L^2(\mathcal{S})$ . These are Hilbert spaces with the standard  $L^2$  inner product  $\langle f, \tilde{f} \rangle_{L^2(\Omega)} = \int_\Omega f(x) \tilde{f}(x) \, dx$ . Moreover,  $\mathcal{R}$  and  $\mathcal{R}^*$  are continuous operators between these Hilbert spaces that are adjoint, i.e.,  $\langle \mathcal{R}f, g \rangle_{L^2(\mathcal{S})} = \langle f, \mathcal{R}^*g \rangle_{L^2(\Omega)}$  for all  $f \in L^2(\Omega)$ ,  $g \in L^2(\mathcal{S})$ .

## 2.2 Discretizations framework

Next, we describe the ray-driven and pixel-driven discretization frameworks as finite rank operators via convolutional discretizations.

We start by discretizing the spatial domain  $\Omega$  and the sinogram domain  $\mathcal{S}$  into ‘pixels’; one can think of data and reconstructions as digital images; see Figure 2. We fix  $N_x \in \mathbb{N}$  and set  $\delta_x := \frac{2}{N_x}$ ,  $[N_x] := \{0, \dots, N_x - 1\}$ . We define the spatial pixel centers  $x_{ij} = (\frac{2i+1}{N_x} - 1, \frac{2j+1}{N_x} - 1) = ((i + \frac{1}{2})\delta_x - 1, (j + \frac{1}{2})\delta_x - 1)$  for  $i, j \in [N_x]$  and  $X_{ij} = x_{ij} + [-\frac{\delta_x}{2}, \frac{\delta_x}{2}]^2$  denotes the corresponding squared (spatial) pixel with side-length (resolution)  $\delta_x$ . We consider a finite number of angles  $\phi_0 < \dots < \phi_{N_\phi-1} \in [0, \pi[$  and associate them with the angular pixel  $\Phi_q = [\frac{\phi_{q-1} + \phi_q}{2}, \frac{\phi_q + \phi_{q+1}}{2}]$  for  $q \in [N_\phi]$ , where we understand  $\phi_{-1} = \phi_{N_\phi-1} - \pi$  and  $\phi_{N_\phi} = \phi_0 + \pi$ . Correspondingly, we set  $\delta_\phi = \max_{q \in [N_\phi]} |\Phi_q|$ . Note that  $\Phi_0$  and  $\Phi_{N_\phi-1}$  are not necessarily in  $[0, \pi[$ , but we can tacitly assume so below (see Remark 1). For the sake of readability, we write  $\vartheta_q$  for the unit vector  $\vartheta_{\phi_q}$  associated with the angle  $\phi_q$ . Similarly, we assume a fixed number  $N_s \in \mathbb{N}$  of

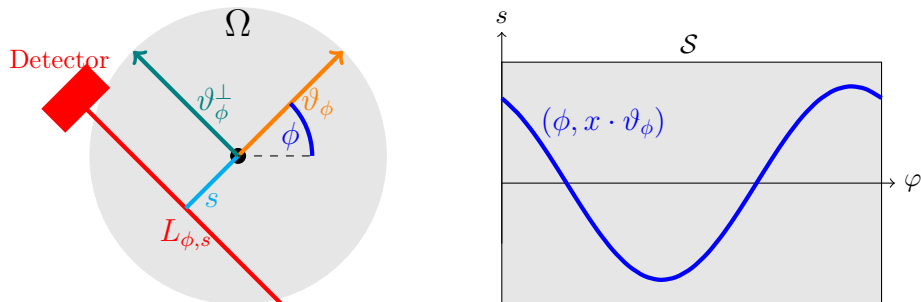


**Fig. 1.** On the left, an illustration of the  $L_{\phi,s}$  geometry as a straight line in direction  $\vartheta_\phi^\perp$  with normal distance to the center  $s$ . On the right, an illustration of the backprojection, where for fixed  $x$  we integrate along a sine-shaped trajectory (representing all lines passing through  $x$ ) in the sinogram domain.

detector pixels and set  $\delta_s = \frac{2}{N_s}$ . The associated equispaced detector pixels are  $S_p := s_p + [-\frac{\delta_s}{2}, \frac{\delta_s}{2}[$  for  $p \in [N_s]$  with centers  $s_p = \frac{2p+1}{N_s} - 1 = (p + \frac{1}{2})\delta_s - 1$ .

Hence, we have discretized the domain  $\Omega$  into a Cartesian  $N_x \times N_x$  grid with (spatial) resolution  $\delta_x$ , while the sinogram space is discretized as an  $N_\phi \times N_s$  grid of rectangular pixels  $\Phi_q \times S_p$  for  $q \in [N_\phi]$  and  $p \in [N_s]$ , i.e., with angular resolution  $\delta_\phi$  and detector resolution  $\delta_s$ ; see Figure 2. We notationally combine all these resolutions to  $\delta = (\delta_x, \delta_\phi, \delta_s) \in \mathbb{R}^+ \times \mathbb{R}^+ \times \mathbb{R}^+$ , and  $N_x, N_\phi$  and  $N_s$  are tacitly chosen accordingly.

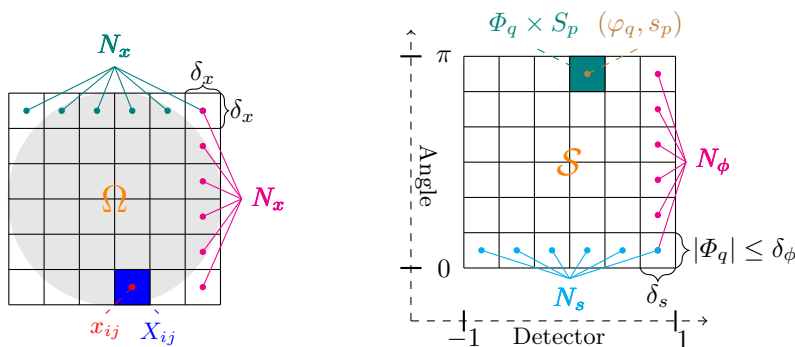


**Fig. 2.** On the left, the discretization of the spatial domain  $\Omega$  into pixels  $X_{ij}$  with width  $\delta_x \times \delta_x$  is depicted. On the right, the discretization of the sinogram domain  $\mathcal{S}$  into pixels  $\Phi_q \times S_p$  of width  $|\Phi_q| \times \delta_s$  is shown.

One can naturally associate pixel values of an image representing  $f \in L^2(\Omega)$  with average values  $f_{ij} := \frac{1}{\delta_x^2} \int_{X_{ij}} f(x) dx$  and functions  $f_\delta = \sum_{i,j=0}^{N_x-1} f_{ij} u_{ij}$  in  $U_\delta := \text{span}\{u_{ij}\}_{i,j \in [N_x]} \hat{=} \mathbb{R}^{N_x^2}$  with  $u_{ij} := \chi_{X_{ij}} - \frac{1}{2} \chi_{\partial X_{ij}}$  where  $\chi_M(x)$  equals 1 if  $x \in M$  and zero otherwise, and  $\partial X_{ij}$  denotes the boundary of  $X_{ij}$ . (In other words,  $u_{ij}$  attains the value 1 inside  $X_{ij}$ ,  $\frac{1}{2}$  on its boundary and zero otherwise.) Similarly, we can consider sinogram images as functions  $g_\delta \in V_\delta := \text{span}\{v_{qp}\}_{q \in [N_\phi], p \in [N_s]} \hat{=} \mathbb{R}^{N_\phi \times N_s}$  with  $v_{qp} := \chi_{\Phi_q \times S_p}$  and the coefficients  $g_{qp}$  are again average values on pixels.

Discretizations of  $\mathcal{R}$  translate to a matrix-vector multiplication with the matrix  $A \in \mathbb{R}^{(N_\phi \cdot N_s) \times N_x^2}$  mapping from  $U_\delta$  to  $V_\delta$  (we think of the pixel values  $(f_{ij})_{i,j \in [N_x]}$  and  $(g_{qp})_{qp}$  as vectors). In practical implementations, these matrices are rarely saved (due to memory constraints). Rather, matrix-free formulations are employed, i.e., the relevant matrix entries are calculated when needed and discarded afterward. The matrix entries  $A_{qpij}$  (the combination of  $q$  and  $p$  determines a row, while  $i$  and  $j$  determine a column) represent the weight attributed to a pixel  $X_{ij}$  in the calculation for  $L_{\phi_q, s_p}$ . In order to compute  $[\mathcal{R}f](\phi, s)$  for a specific pair  $(\phi, s)$ , one has to take relatively few values (the values along  $L_{\phi, s}$ ) into account; therefore, also the  $A_{qpij}$  should be non-zero only for pixels that are close to  $L_{\phi_q, s_p}$ . This way, the matrix  $A$  is relatively sparse, which is of practical importance. Next, we define suitable weights related to common discretization schemes.

**Definition 3 (Weight functions).** *Given  $\delta$  and  $\phi \in [0, \pi[$ , we set  $\bar{s}(\phi) := \frac{\delta_x}{2} (|\cos(\phi)| + |\sin(\phi)|)$ ,  $\underline{s}(\phi) := \frac{\delta_x}{2} (|\cos(\phi)| - |\sin(\phi)|)$  and  $\kappa(\phi) := \min \left\{ \frac{1}{|\cos(\phi)|}, \frac{1}{|\sin(\phi)|} \right\}$ . We define the ray-driven weight function for  $t \in \mathbb{R}$  according to*

$$\omega_{\delta_x}^{\text{rd}}(\phi, t) := \frac{1}{\delta_x} \begin{cases} \kappa(\phi) & \text{if } |t| < \underline{s}(\phi), \\ \frac{\bar{s}(\phi) - |t|}{\delta_x |\cos(\phi) \sin(\phi)|} & \text{if } |t| \in [\underline{s}(\phi), \bar{s}(\phi)], \\ \frac{1}{2} & \text{if } \phi \in \frac{\pi}{2} \mathbb{Z} \text{ and } |t| = \bar{s}(\phi), \\ 0 & \text{else,} \end{cases} \quad (3)$$

where  $\frac{\pi}{2} \mathbb{Z}$  denotes all multiples of  $\frac{\pi}{2}$ . Moreover, we define the pixel-driven weight function to be

$$\omega_{\delta_s}^{\text{pd}}(\phi, t) = \omega_{\delta_s}^{\text{pd}}(t) := \frac{1}{\delta_s^2} \max\{\delta_s - |t|, 0\} \quad \text{for } t \in \mathbb{R}, \phi \in [0, \pi[. \quad (4)$$

The ray-driven method (as described in the literature) uses the intersection lengths of lines and pixels as weights, i.e.,  $A_{qpij} = \mathcal{H}^1(X_{ij} \cap L_{\phi_q, s_p})$ , computed in an iterative manner following the ray [6]; see Figure 4. The value  $\delta_x^2 \omega_{\delta_x}^{\text{rd}}(\phi_q, x_{ij} \cdot \vartheta_q - s_p)$  is a closed-form expression of this weight (see Lemma 1) required for the more structured analysis we will execute in Section 3. The special case  $\phi \in \frac{\pi}{2} \mathbb{Z}$  and  $|t| = \bar{s}(\phi)$  in (3) relates to when  $L_{\phi, s} \cap Z = L_{\phi, s} \cap \partial Z$  is one side of the pixel  $X_{ij}$ . To avoid counting said edge twice (once for each of the pixels

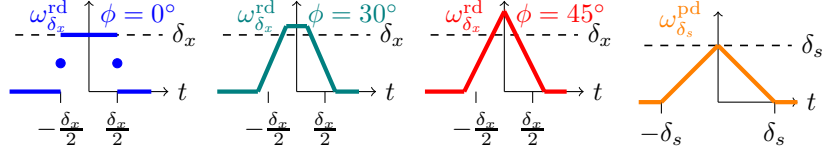


**Fig. 3.** Depiction of the ray-driven weight function  $t \mapsto \delta_x^2 \omega_{\delta_x}^{\text{rd}}(\phi, t)$  for fixed  $\phi \in \{0^\circ, 30^\circ, 45^\circ\}$ . These are trapezoid functions (like the  $30^\circ$  case), whose incline, height, and width depend on  $\phi$ , with  $\phi = 0^\circ$  and  $\phi = 45^\circ$  as the extreme cases. On the right, a depiction of the pixel-driven weight function  $t \mapsto \delta_s^2 \omega_{\delta_s}^{\text{pd}}(t)$  independent of  $\phi$ .

containing the edge), we attribute half the intersection length to the two pixels sharing this side. This choice is somewhat arbitrary; what matters is that they sum up to 1.

The pixel-driven weight is such that there are at most two  $p$  (for fixed  $q \in [N_\phi]$  and  $i, j \in [N_x]$ ) such that  $A_{qp} \neq 0$ , and whose sum equals 1 (see Lemma 2). One can imagine the pixel's contribution is distributed onto the two closest lines; one speaks of antepolation. Moreover, this results in a backprojection with linear interpolation (with respect to the detector dimension) of the closest relevant detector pixels; see Figure 4.

**Lemma 1 (Closed form of the intersection length).** *Given  $\phi \in [0, \pi[$  and  $s \in \mathbb{R}$ , we have*

$$\delta_x^2 \omega_{\delta_x}^{\text{rd}}(\phi, x_{ij} \cdot \vartheta_\phi - s) = \mathcal{H}^1(L_{\phi,s} \cap X_{ij}) - \frac{1}{2} \mathcal{H}^1(L_{\phi,s} \cap \partial X_{ij}). \quad (5)$$

The proof of this statement is quite geometric with multiple case distinctions and is found in the Appendix.

In order to compare the matrices representing discretizations with  $\mathcal{R}$  and  $\mathcal{R}^*$ , we next reinterpret them as finite rank operators mapping from  $L^2(\Omega)$  to  $L^2(\mathcal{S})$  or vice versa. More precisely, they map into  $U_\delta$  and  $V_\delta$  spanned by  $u_{ij} := \chi_{X_{ij}} - \frac{1}{2} \chi_{\partial X_{ij}}$  and  $v_{qp} := \chi_{\Phi_q \times S_p}$  for  $i, j \in [N_x]$ ,  $q \in [N_\phi]$  and  $p \in [N_s]$ .

**Definition 4 (Convolutional discretizations).** *Given  $\delta$ , the ray-driven Radon transform  $\mathcal{R}_\delta^{\text{rd}}$  and the pixel-driven Radon transform  $\mathcal{R}_\delta^{\text{pd}}$  are defined as special cases of the convolutional Radon transform  $\mathcal{R}_\omega: L^2(\Omega) \rightarrow L^2(\mathcal{S})$ , such that, for a function  $f \in L^2(\Omega)$ ,*

$$[\mathcal{R}_\omega f](\phi, s) := \sum_{q=0}^{N_\phi-1} \sum_{p=0}^{N_s-1} v_{qp}(\phi, s) \sum_{i,j=0}^{N_x-1} \omega(\phi_q, x_{ij} \cdot \vartheta_q - s_p) \int_{X_{ij}} f(x) dx, \quad (6)$$

where  $\omega$  is replaced with  $\omega_{\delta_x}^{\text{rd}}$  or  $\omega_{\delta_s}^{\text{pd}}$ , respectively. The corresponding ray-driven or pixel-driven backprojections  $\mathcal{R}_\delta^{\text{rd}*}$  and  $\mathcal{R}_\delta^{\text{pd}*}$  are special cases of the convolutional

backprojection  $\mathcal{R}_\omega^*: L^2(\mathcal{S}) \rightarrow L^2(\Omega)$  according to

$$[\mathcal{R}_\omega^* g](x) := \sum_{i,j=0}^{N_x-1} u_{ij}(x) \sum_{q=0}^{N_\phi-1} \sum_{p=0}^{N_s-1} \omega(\phi_q, x_{ij} \cdot \vartheta_q - s_p) \int_{\Phi_q \times S_p} g(\phi, s) d(\phi, s) \quad (7)$$

for  $g \in L^2(\mathcal{S})$  when setting  $\omega$  to  $\omega_{\delta_x}^{\text{rd}}$  or  $\omega_{\delta_s}^{\text{pd}}$ , respectively. (Note that here we tacitly restrict the functions  $u_{ij}$  to  $\Omega$ .)

Note that the output of these operators is constant on the pixels, thus mapping  $U_\delta$  to  $V_\delta$  or vice-versa, and the corresponding pixel values (coefficients) are

$$[R_\omega f]_{qp} = \delta_x^2 \sum_{i,j=0}^{N_x-1} \omega(\phi_q, x_{ij} \cdot \vartheta_q - s_p) f_{ij}, \quad (8)$$

$$[R_\omega^* g]_{ij} = \delta_s \sum_{q=0}^{N_\phi-1} |\Phi_q| \sum_{p=0}^{N_s-1} \omega(\phi_q, x_{ij} \cdot \vartheta_q - s_p) g_{qp}, \quad (9)$$

which coincide with the classical definitions of the ray-driven and pixel-driven methods as matrix-vector multiplications.

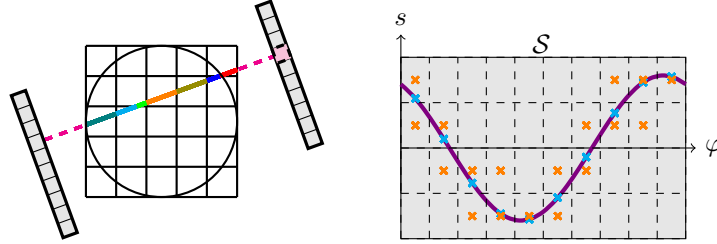


**Fig. 4.** Illustration of the ray-driven forward (left) and the pixel-driven backprojection (right). In the former, the integration along a straight line is the sum of integrals along the intersections with pixels (colored segments), whose contribution is the intersection lengths. The pixel-driven backprojection discretizes the angular integral (2) (along the violet curve  $x \cdot \vartheta_\phi$ ) by a finite sum of angular evaluations  $x \cdot \vartheta_q$  (the cyan dots), that are approximated via linear interpolation in the detector dimension (using the neighboring orange pixel centers).

*Remark 2.* Obviously,  $u_{ij} = \chi_{X_{ij}} - \frac{1}{2}\chi_{X_{ij}} = \chi_{X_{ij}}$  in a (Lebesgue) almost everywhere sense. Thus, also  $\mathcal{R}(\chi_{X_{ij}} - \frac{1}{2}\chi_{X_{ij}}) = \mathcal{R}\chi_{X_{ij}}$  almost everywhere and values of Lebesgue null sets are irrelevant. However, if we evaluate the Radon transform pointwise for discretization purposes, suddenly Lebesgue null sets in  $\Omega$  and  $\mathcal{S}$  could be relevant. Rather, due to the Radon transform's relation to the one-dimensional Hausdorff measure  $\mathcal{H}^1$ , we define  $u_{ij}$  in an  $\mathcal{H}^1$  almost everywhere sense, with the value 1 in the interior of  $X_{ij}$ ,  $\frac{1}{2}$  on the boundary. The



corners are a bit of a special case as we would actually like the values to be  $\frac{1}{4}$ , but these are an  $\mathcal{H}^1$  null set and thus of no consequence. Analogously, functions  $f_\delta \in U_\delta$  are understood as being defined  $\mathcal{H}^1$  almost everywhere. Note that  $U_\delta$  is not a native subset of  $L^2(\Omega)$ , but of  $L^2([-1, 1]^2)$ . We tacitly extend the definition of the Radon transform in (1) to  $L^2([-1, 1]^2)$  where necessary.

### 3 Convergence Analysis

These discretization frameworks have been known for decades (at least as practical implementations), but no rigorous convergence results were presented. Our interpretation of discretizations as finite rank operators (via convolutional discretizations) allows the comparison of ‘continuous’ operators with their discretizations. Those comparisons culminate in Theorem 1, which complements anecdotal reports on the performance of discretization approaches by describing convergence in the strong operator topology (SOT).

**Theorem 1 (Convergence in the strong operator topology).**

Let  $(\delta^n)_{n \in \mathbb{N}} = (\delta_x^n, \delta_\phi^n, \delta_s^n)_{n \in \mathbb{N}}$  be a sequence of discretization parameters with  $\delta^n \xrightarrow{n \rightarrow \infty} 0$  (componentwise) and let  $c > 0$  be a constant. If  $\frac{\delta_s^n}{\delta_x^n} < c$  for all  $n \in \mathbb{N}$ , then, for any  $f \in L^2(\Omega)$ , we have

$$\lim_{n \rightarrow \infty} \|\mathcal{R}f - \mathcal{R}_{\delta^n}^{\text{rd}} f\|_{L^2(\mathcal{S})} = 0. \quad (\text{conv}^{\text{rd}})$$

If the sequence  $(\delta_n)_{n \in \mathbb{N}}$  satisfies  $\frac{\delta_s^n}{\delta_x^n} \xrightarrow{n \rightarrow \infty} 0$ , then, for each  $g \in L^2(\mathcal{S})$ , we have

$$\lim_{n \rightarrow \infty} \|\mathcal{R}^* g - \mathcal{R}_{\delta^n}^{\text{rd}*} g\|_{L^2(\Omega)} = 0. \quad (\text{conv}^{\text{rd}*})$$

If  $\frac{\delta_x^n}{\delta_s^n} \leq c$  for all  $n \in \mathbb{N}$ , then, for each  $g \in L^2(\mathcal{S})$ , we have

$$\lim_{n \rightarrow \infty} \|\mathcal{R}^* g - \mathcal{R}_{\delta^n}^{\text{pd}*} g\|_{L^2(\Omega)} = 0. \quad (\text{conv}^{\text{pd}*})$$

*Remark 3.* Note that both  $(\text{conv}^{\text{rd}})$  and  $(\text{conv}^{\text{pd}*})$  are applicable in the case  $\delta_x^n \approx \delta_s^n$ . Hence, using the rd-pd\* approach for balanced resolutions is indeed justified in the sense that we have pointwise convergence of the operators (SOT). In the unbalanced case  $\frac{\delta_s^n}{\delta_x^n} \rightarrow 0$ , also the rd-rd\* approach is justified in the sense of SOT. Note that the convergence described in Theorem 1 is not necessarily uniform, i.e., the speed of convergence could depend significantly on the specific functions  $f$  and  $g$  considered and might potentially get arbitrarily slow.

In order to prove Theorem 1, we need to discuss some additional properties of the weight functions yielding exact approximations in certain situations.

**Lemma 2 (Exact weights).** Let  $f \in L^2(\Omega)$ , and given  $\delta$ , let  $f_\delta = \sum_{i,j=0}^{N_x-1} f_{ij} u_{ij} \in U_\delta$  with  $f_{ij} = \frac{1}{\delta_x^2} \int_{X_{ij}} f \, dx$  (the projection of  $f$  onto  $U_\delta$ ). Let  $(\phi, s) \in \mathcal{S}$  and let  $\hat{q} \in [N_\phi]$  and  $\hat{p} \in [N_s]$  be such that  $(\phi, s) \in \Phi_{\hat{q}} \times S_{\hat{p}}$ . Then, we have

$$[\mathcal{R}_\delta^{\text{rd}} f](\phi, s) = [\mathcal{R}_\delta^{\text{rd}} f_\delta](\phi_{\hat{q}}, s_{\hat{p}}) = [\mathcal{R} f_\delta](\phi_{\hat{q}}, s_{\hat{p}}). \quad (\text{exact}^{\text{rd}})$$

Note that here  $f_\delta \in U_\delta$  is understood as defined  $\mathcal{H}^1$  almost everywhere (see Remark 2); thus  $[\mathcal{R} f_\delta](\phi_{\hat{q}}, s_{\hat{p}})$  is well-defined. Moreover, for fixed  $\hat{i}, \hat{j} \in [N_x]$ , we have

$$\sum_{p=0}^{N_s-1} \omega_{\delta_s}^{\text{pd}}(x_{\hat{i}\hat{j}} \cdot \vartheta_{\hat{q}} - s_p) \quad \left\{ \begin{array}{ll} = \frac{1}{\delta_s} & \text{if } x_{\hat{i}\hat{j}} \cdot \vartheta_{\hat{q}} \in [s_0, s_{N_s-1}], \\ < \frac{1}{\delta_s} & \text{else,} \end{array} \right. \quad (\text{intpol}^{\text{pd}})$$

with exactly two non-zero summands  $\hat{p}$  and  $\hat{p} + 1$  if  $x_{\hat{i}\hat{j}} \cdot \vartheta_{\hat{q}} \in ]s_{\hat{p}}, s_{\hat{p}+1}[$  and a single non-zero summand  $\hat{p}$  if  $x_{\hat{i}\hat{j}} \cdot \vartheta_{\hat{q}} = s_{\hat{p}}$ . In the case  $x_{\hat{i}\hat{j}} \cdot \vartheta_{\hat{q}} \notin [s_0, s_{N_s-1}]$  (i.e.,  $|x_{\hat{i}\hat{j}} \cdot \vartheta_{\hat{q}}| > 1 - \frac{\delta_s}{2}$ ), there is at most one non-zero summand.

In other words, the ray-driven Radon transform is exact on  $U_\delta$  for evaluation on sinogram pixel centers, and coincides with  $\mathcal{R}_\delta^{\text{rd}} f$  when  $f_\delta$  is the projection of  $f$  onto  $U_\delta$ . In contrast, the sum of pixel-driven weights equals  $\frac{1}{\delta_s}$  while inside the detector range, which results in an interpolation effect in the backprojection.

*Proof (Lemma 2).* ( $\text{exact}^{\text{rd}}$ ): We consider  $f_\delta = \sum_{i,j=0}^{N_x-1} f_{ij} u_{ij} \in U_\delta$  with the coefficients  $f_{ij} = \frac{1}{\delta_x^2} \int_{X_{ij}} f_\delta(x) dx$ . We have  $[\mathcal{R}_\delta^{\text{rd}} f](\phi, s) = [\mathcal{R}_\delta^{\text{rd}} f](\phi_{\hat{q}}, s_{\hat{p}})$  for  $(\phi, s) \in \Phi_{\hat{q}} \times S_{\hat{p}}$  (these are constant functions on the sinogram pixels). Since  $\int_{X_{ij}} f dx = \int_{X_{ij}} f_\delta dx$ , we have  $[\mathcal{R}_\delta^{\text{rd}} f](\phi, s) = [\mathcal{R}_\delta^{\text{rd}} f_\delta](\phi_{\hat{q}}, s_{\hat{p}})$  per definition.

Moreover, we calculate

$$\begin{aligned} [\mathcal{R} f_\delta](\phi_{\hat{q}}, s_{\hat{p}}) &\stackrel{\text{lin}}{=} \sum_{i,j=0}^{N_x-1} f_{ij} [\mathcal{R} u_{ij}](\phi_{\hat{q}}, s_{\hat{p}}) \\ &\stackrel{\text{per def}}{=} \sum_{i,j=0}^{N_x-1} f_{ij} \left( \int_{\mathbb{R}^2} \chi_{X_{ij}} d\mathcal{H}^1 \llcorner L_{\phi_{\hat{q}}, s_{\hat{p}}} - \frac{1}{2} \int_{\mathbb{R}^2} \chi_{\partial X_{ij}} d\mathcal{H}^1 \llcorner L_{\phi_{\hat{q}}, s_{\hat{p}}} \right) \\ &= \sum_{i,j=0}^{N_x-1} f_{ij} \left( \mathcal{H}^1(L_{\phi_{\hat{q}}, s_{\hat{p}}} \cap X_{ij}) - \frac{1}{2} \mathcal{H}^1(L_{\phi_{\hat{q}}, s_{\hat{p}}} \cap \partial X_{ij}) \right) \\ &\stackrel{(5)}{=} \sum_{i,j=0}^{N_x-1} f_{ij} \delta_x^2 \omega_{\delta_x}^{\text{rd}}(\phi_{\hat{q}}, x_{ij} \cdot \vartheta_{\hat{q}} - s_{\hat{p}}) \stackrel{\text{per def}}{=} [\mathcal{R}_\delta^{\text{rd}} f_\delta](\phi_{\hat{q}}, s_{\hat{p}}). \end{aligned}$$

( $\text{intpol}^{\text{pd}}$ ): Note that  $\omega_{\delta_s}^{\text{pd}}(t) \neq 0$  iff  $t \in ]-\delta_s, \delta_s[$ . If  $x_{\hat{i}\hat{j}} \cdot \vartheta_{\hat{q}} = s_{\hat{p}}$  for some  $\hat{p} \in [N_s]$ , then  $\omega_{\delta_s}^{\text{pd}}(x_{\hat{i}\hat{j}} \cdot \vartheta_{\hat{q}} - s_{\hat{p}}) = \omega_{\delta_s}^{\text{pd}}(0) = \frac{1}{\delta_s}$  and  $|x_{\hat{i}\hat{j}} \cdot \vartheta_{\hat{q}} - s_p| = |s_{\hat{p}} - s_p| \geq \delta_s$  for  $p \neq \hat{p}$  and therefore  $\omega_{\delta_s}^{\text{pd}}(x_{\hat{i}\hat{j}} \cdot \vartheta_{\hat{q}} - s_p) = 0$ , implying ( $\text{intpol}^{\text{pd}}$ ).

If  $x_{\hat{i}\hat{j}} \cdot \vartheta_{\hat{q}} \in [s_0, s_{N_s-1}]$ , but  $x_{\hat{i}\hat{j}} \cdot \vartheta_{\hat{q}} \neq s_p$  for all  $p \in [N_s]$ , then there is a  $\hat{p} \in [N_s - 1]$  with  $x_{\hat{i}\hat{j}} \cdot \vartheta_{\hat{q}} \in ]s_{\hat{p}}, s_{\hat{p}+1}[$ . Recall  $s_p = s_0 + p\delta_s$ , and consequently

$$|x_{\hat{i}\hat{j}} \cdot \vartheta_{\hat{q}} - s_p| = \min_{p^* \in \{\hat{p}, \hat{p}+1\}} |p - p^*| \delta_s + |x_{\hat{i}\hat{j}} \cdot \vartheta_{\hat{q}} - s_{p^*}| \geq \delta_s \quad (10)$$

for  $p \notin \{\hat{p}, \hat{p} + 1\}$  and thus  $\omega_{\delta_s}^{\text{pd}}(\phi_{\hat{q}}, x_{i\hat{j}} \cdot \vartheta_{\hat{q}} - s_p) = 0$ . We set  $t = x_{i\hat{j}} \cdot \vartheta_{\hat{q}} - s_{\hat{p}+1} \in ] - \delta_s, 0[$ , and  $t + \delta_s = x_{i\hat{j}} \cdot \vartheta_{\hat{q}} - s_{\hat{p}+1} + \delta_s = x_{i\hat{j}} \cdot \vartheta_{\hat{q}} - s_{\hat{p}}$ . Then,

$$\begin{aligned} \delta_s^2 \sum_{p=0}^{N_s-1} \omega_{\delta_s}^{\text{pd}}(x_{i\hat{j}} \cdot \vartheta_{\hat{q}} - s_p) &= (\omega_{\delta_s}^{\text{pd}}(x_{i\hat{j}} \cdot \vartheta_{\hat{q}} - s_{\hat{p}}) + \omega_{\delta_s}^{\text{pd}}(x_{i\hat{j}} \cdot \vartheta_{\hat{q}} - s_{\hat{p}+1})) \delta_s^2 \\ &= (\omega_{\delta_s}^{\text{pd}}(t) + \omega_{\delta_s}^{\text{pd}}(t + \delta_s)) \delta_s^2 \stackrel{\text{per}}{\underset{\text{def}}{=} } \delta_s + t + \delta_s - \delta_s - t = \delta_s, \end{aligned} \quad (11)$$

implying (intpol<sup>pd</sup>).

If  $x_{i\hat{j}} \cdot \vartheta_{\hat{q}} \notin [s_0, s_{N_s-1}]$ , there is at most one non-zero summand in (intpol<sup>pd</sup>), which is also bounded by  $\frac{1}{\delta_s}$ , implying the claim.

In order to obtain suitable estimates, we require knowledge on the behavior of the sum of weights over all spatial or detector pixels.

**Lemma 3 (Sums of weights).** *Given  $\delta, \hat{i}, \hat{j} \in [N_x]$ ,  $\hat{q} \in [N_\phi]$  and  $\hat{p} \in [N_s]$ , the following hold:*

$$\sum_{i,j=0}^{N_x-1} \omega_{\delta_x}^{\text{rd}}(\phi_{\hat{q}}, x_{ij} \cdot \vartheta_{\hat{q}} - s_{\hat{p}}) \leq \frac{\sqrt{8}}{\delta_x^2}. \quad (\Sigma_{ij}^{\text{rd}})$$

$$\sum_{p=0}^{N_s-1} \omega_{\delta_x}^{\text{rd}}(\phi_{\hat{q}}, x_{i\hat{j}} \cdot \vartheta_{\hat{q}} - s_p) \in \begin{cases} \frac{1}{\delta_s} + [-\frac{\sqrt{8}}{\delta_x}, \frac{\sqrt{8}}{\delta_x}] & \text{if } |x_{i\hat{j}} \cdot \vartheta_{\hat{q}}| \leq 1 - \frac{\delta_x}{\sqrt{2}}, \\ [0, \frac{1}{\delta_s} + \frac{\sqrt{8}}{\delta_x}] & \text{otherwise.} \end{cases} \quad (\Sigma_p^{\text{rd}})$$

$$\sum_{i,j=0}^{N_x-1} \omega_{\delta_s}^{\text{pd}}(x_{ij} \cdot \vartheta_{\hat{q}} - s_{\hat{p}}) \leq \left\lceil \frac{\delta_s}{\delta_x} \right\rceil \frac{4\sqrt{2}}{\delta_x \delta_s}, \quad (\Sigma_{ij}^{\text{pd}})$$

where  $\lceil t \rceil := \min\{n \in \mathbb{N} \mid t \leq n\}$ .

*Proof.* ( $\Sigma_{ij}^{\text{rd}}$ ): According to Lemma 2's (exact<sup>rd</sup>) for  $f_\delta = \sum_{i,j=0}^{N_x-1} 1u_{ij} \in U_\delta$  (constantly one), we see that

$$\delta_x^2 \sum_{i,j=0}^{N_x-1} \omega_{\delta_x}^{\text{rd}}(\phi_{\hat{q}}, x_{ij} \cdot \vartheta_{\hat{q}} - s_{\hat{p}}) \stackrel{\text{per}}{\underset{\text{def}}{=} } [\mathcal{R}_\delta^{\text{rd}} f_\delta](\phi_{\hat{q}}, s_{\hat{p}}) \stackrel{(\text{exact}^{\text{rd}})}{=} [\mathcal{R} f_\delta](\phi_{\hat{q}}, s_{\hat{p}}) \leq \sqrt{8},$$

where the last estimate is simply the maximal length ( $\sqrt{8}$ ) of the ray in  $[-1, 1]^2$  times the maximal value of  $f_\delta$  (being 1).

( $\Sigma_p^{\text{rd}}$ ): We note that the function  $G(t) := \omega_{\delta_x}^{\text{rd}}(\phi_{\hat{q}}, t)$  is monotone for  $t \geq 0$  and  $t \leq 0$ , respectively (see Figure 3). Moreover,  $G(t) \in [0, \frac{\sqrt{2}}{\delta_x}]$  for all  $t \in \mathbb{R}$ ,  $\text{supp}(G) \subset [-\frac{\delta_x}{\sqrt{2}}, \frac{\delta_x}{\sqrt{2}}]$  and  $\int_{\mathbb{R}} G(t) dt = 1$  (using (5) and Fubini's theorem). For such a function  $G$ , a Riemann sum with stepsize  $\delta_s$  can approximate the integral of  $G$  up to  $2\delta_s \max_t G(t)$ , and therefore

$$\left| \delta_s \sum_{k=-\infty}^{\infty} \omega_{\delta_x}^{\text{rd}}(\phi_{\hat{q}}, t_0 + k\delta_s) - \underbrace{\int_{\mathbb{R}} \omega_{\delta_x}^{\text{rd}}(\phi_{\hat{q}}, t) dt}_{=1} \right| \leq \sqrt{8} \frac{\delta_s}{\delta_x} \quad (12)$$

for any  $t_0 \in \mathbb{R}$ . Setting  $t_0 = s_0 - x_{i\hat{j}} \cdot \vartheta_{\hat{q}}$ , we note  $t_0 + k\delta_s = s_k - x_{i\hat{j}} \cdot \vartheta_{\hat{q}}$  for  $k \in [N_s]$ . If  $|x_{i\hat{j}} \cdot \vartheta_{\hat{q}}| < 1 - \frac{\delta_x}{\sqrt{2}}$  and  $k \notin [N_s]$ , we have

$$|s_0 + k\delta_s - x_{i\hat{j}} \cdot \vartheta_{\hat{q}}| \geq |s_0 + k\delta_s| - |x_{i\hat{j}} \cdot \vartheta_{\hat{q}}| \geq \left(1 + \frac{\delta_s}{2}\right) - \left(1 - \frac{\delta_x}{\sqrt{2}}\right) \geq \frac{\delta_x}{\sqrt{2}}, \quad (13)$$

implying  $\omega_{\delta_x}^{\text{rd}}(\phi_{\hat{q}}, t_0 + k\delta_s) = 0$ , i.e., all summands in (12) for  $k \notin [N_s]$  vanish. Thus, (12) but only with the summands for  $k \in [N_s]$  and  $t_0 + k\delta_s = s_k - x_{i\hat{j}} \cdot \vartheta_{\hat{q}}$  yields  $(\sum_p^{\text{rd}})$ .

We achieve the estimate  $(\sum_p^{\text{rd}})$  if  $|x_{i\hat{j}} \cdot \vartheta_{\hat{q}}| \geq 1 - \frac{\delta_x}{\sqrt{2}}$  by reformulation of (12) according to

$$\sum_{p=0}^{N_s-1} \omega_{\delta_x}^{\text{rd}}(\phi_{\hat{q}}, x_{i\hat{j}} \cdot \vartheta_{\hat{q}} - s_p) \leq \sum_{k=-\infty}^{\infty} \omega_{\delta_x}^{\text{rd}}(\phi_{\hat{q}}, t_0 + k\delta_s) \leq \frac{1}{\delta_s} + \frac{\sqrt{8}}{\delta_x}, \quad (14)$$

where we used that all summands are non-negative.

$(\sum_{ij}^{\text{pd}})$ : We wish to count the set  $\{ij \mid |x_{ij} \cdot \vartheta_{\hat{q}} - s_{\hat{p}}| \leq \delta_s\}$ , as those are the pixels with non-zero contributions  $\omega_{\delta_s}^{\text{pd}}(x_{ij} \cdot \vartheta_{\hat{q}} - s_{\hat{p}})$  to  $(\sum_{ij}^{\text{pd}})$  (as  $\text{supp}(\omega_{\delta_s}^{\text{pd}}) \subset [-\delta_s, \delta_s]$ ). We assume w.l.o.g.  $\phi_{\hat{q}} \in [-\frac{\pi}{4}, -\frac{\pi}{4}]$  (and thus  $|\sin(\phi_{\hat{q}})| \geq \frac{1}{\sqrt{2}}$ ). Fixing  $\hat{i}$ , the inequality  $\delta_s > |s_{\hat{p}} - x_{i\hat{j}} \cdot \vartheta_{\hat{q}}| = |s_{\hat{p}} - x_{i0} \cdot \vartheta_{\hat{q}} - j\delta_x \sin(\phi_{\hat{q}})|$  has at most  $2\sqrt{2}\lceil \frac{\delta_s}{\delta_x} \rceil$  solutions for  $j$  (there may be one even if  $\delta_s \ll \delta_x$ ). Hence, summing up for all  $\hat{i} \in [N_x]$ , we have  $2\sqrt{2}N_x \lceil \frac{\delta_s}{\delta_x} \rceil$  relevant pixels (and  $N_x = \frac{2}{\delta_x}$ ). The sum  $(\sum_{ij}^{\text{pd}})$  can thus be estimated by the number of non-zero summands  $(\frac{4\sqrt{2}}{\delta_x} \lceil \frac{\delta_s}{\delta_x} \rceil)$  times the maximum of  $\omega_{\delta_s}^{\text{pd}} (= \frac{1}{\delta_s})$ , yielding  $(\sum_{ij}^{\text{pd}})$ .

Thanks to these estimates, we can show next that  $\mathcal{R}_{\delta}^{\text{rd}}$  and  $\mathcal{R}_{\delta}^{\text{pd}}$  have bounded operator norms for reasonable choices of  $\delta$ . This is certainly a necessary condition to achieve convergence in the strong operator topology in Theorem 1 due to the uniform boundedness principle. On the other hand, uniform boundedness will be a crucial tool in proving Theorem 1.

**Lemma 4 (Uniformly bounded discretization).** *Let  $c > 0$  be a constant. Then,*

$$\sup \left\{ \|\mathcal{R}_{\delta}^{\text{rd}}\| \mid \delta = (\delta_x, \delta_{\phi}, \delta_s) \in (\mathbb{R}^+)^3 : \frac{\delta_s}{\delta_x} \leq c \right\} < \infty, \quad (\text{BD}^{\text{rd}})$$

$$\sup \left\{ \|\mathcal{R}_{\delta}^{\text{pd}}\| \mid \delta = (\delta_x, \delta_{\phi}, \delta_s) \in (\mathbb{R}^+)^3 : \frac{\delta_x}{\delta_s} \leq c \right\} < \infty, \quad (\text{BD}^{\text{pd}})$$

where  $\|\cdot\|$  refers to the operator norm for operators from  $L^2(\Omega)$  to  $L^2(\mathcal{S})$ .

*Proof.* ( $\text{BD}^{\text{rd}}$ ): We define the sub-probability (thanks to  $(\sum_{ij}^{\text{rd}})$ ) measure  $\mu_{qp} := \frac{1}{\sqrt{8}} \sum_{i,j=0}^{N_x-1} \omega_{\delta_x}^{\text{rd}}(\phi_q, x_{ij} \cdot \vartheta_q - s_p) \mathcal{L}^2 \llcorner X_{ij}$  with  $\mathcal{L}^2$  the two-dimensional Lebesgue measure. Given  $f \in L^2(\Omega)$ , and using Jensen's inequality for  $\mu_{qp}$ , we have

$$\begin{aligned} \|\mathcal{R}_\delta^{\text{rd}} f\|_{L^2(\mathcal{S})}^2 &\stackrel{\text{per}}{\stackrel{\text{def}}{=}} \sum_{q=0}^{N_\phi-1} \sum_{p=0}^{N_s-1} \delta_s |\Phi_q| \left| \sum_{i,j=0}^{N_x-1} \omega_{\delta_x}^{\text{rd}}(\phi_q, x_{ij} \cdot \vartheta_q - s_p) \int_{X_{ij}} f(x) dx \right|^2 \\ &\stackrel{\text{per}}{\stackrel{\text{def}}{=}} 8 \sum_{q=0}^{N_\phi-1} \sum_{p=0}^{N_s-1} \delta_s |\Phi_q| \left| \int_{\Omega} f(x) d\mu_{qp}(x) \right|^2 \stackrel{\text{Jen}}{\leq} 8 \sum_{q=0}^{N_\phi-1} \sum_{p=0}^{N_s-1} \delta_s |\Phi_q| \int_{\Omega} |f(x)|^2 d\mu_{qp}(x) \\ &\stackrel{\text{per}}{\stackrel{\text{def}}{=}} \sqrt{8} \sum_{i,j=0}^{N_x-1} \int_{X_{ij}} |f(x)|^2 dx \sum_{q=0}^{N_\phi-1} |\Phi_q| \sum_{p=0}^{N_s-1} \delta_s \omega_{\delta_x}^{\text{rd}}(\phi_q, x_{ij} \cdot \vartheta_q - s_p) \\ &\stackrel{(\sum_p^{\text{rd}})}{\leq} \sqrt{8\pi} \left( 1 + \sqrt{8} \frac{\delta_s}{\delta_x} \right) \|f\|_{L^2(\Omega)}^2, \end{aligned}$$

where we used  $\|f\|_{L^2(\Omega)}^2 = \sum_{i,j=0}^{N_x-1} \int_{X_{ij}} |f(x)|^2 dx$  and  $\sum_{q=0}^{N_\phi-1} |\Phi_q| = \pi$ . Consequently,  $\|\mathcal{R}_\delta^{\text{rd}}\|^2 \leq \sqrt{8\pi}(1 + \sqrt{8}c)$  if  $\frac{\delta_s}{\delta_x} \leq c$ .

( $\text{BD}^{\text{pd}}$ ): We define the sub-probability (due to  $(\text{intpo}^{\text{pd}})$ ) measure  $\nu_{ij} := \frac{1}{\pi} \sum_{q=0}^{N_\phi-1} \sum_{p=0}^{N_s-1} \omega_{\delta_s}^{\text{pd}}(x_{ij} \cdot \vartheta_q - s_p) \mathcal{L}^2 \llcorner (\Phi_q \times S_p)$ . Given  $g \in L^2(\mathcal{S})$ , we use Jensen's inequality to get

$$\begin{aligned} \|\mathcal{R}_\delta^{\text{pd}*} g\|_{L^2(\Omega)}^2 &\stackrel{\text{per}}{\stackrel{\text{def}}{=}} \delta_x^2 \sum_{i,j=0}^{N_x-1} \left| \sum_{q=0}^{N_\phi-1} \sum_{p=0}^{N_s-1} \omega_{\delta_s}^{\text{pd}}(x_{ij} \cdot \vartheta_q - s_p) \int_{\Phi_q \times S_p} g(\phi, s) d(\phi, s) \right|^2 \\ &\stackrel{\text{per}}{\stackrel{\text{def}}{=}} \delta_x^2 \pi^2 \sum_{i,j=0}^{N_x-1} \left| \int_{\mathcal{S}} g(\phi, s) d\nu_{ij}(\phi, s) \right|^2 \stackrel{\text{Jen}}{\leq} \delta_x^2 \pi^2 \sum_{i,j=0}^{N_x-1} \int_{\mathcal{S}} |g(\phi, s)|^2 d\nu_{ij}(\phi, s) \\ &\stackrel{\text{per}}{\stackrel{\text{def}}{=}} \delta_x^2 \pi \sum_{i,j=0}^{N_x-1} \left( \sum_{q=0}^{N_\phi-1} \sum_{p=0}^{N_s-1} \omega_{\delta_s}^{\text{pd}}(x_{ij} \cdot \vartheta_q - s_p) \int_{\Phi_q \times S_p} |g(\phi, s)|^2 d(\phi, s) \right). \end{aligned} \tag{15}$$

Pulling the sum  $\sum_{i,j=0}^{N_x-1}$  into the other summands, using  $(\sum_{ij}^{\text{pd}})$  and  $\|g\|_{L^2(\mathcal{S})}^2 = \sum_{q=0}^{N_\phi-1} \sum_{p=0}^{N_s-1} \int_{\Phi_q \times S_p} |g|^2 d(\phi, s)$ , we see that  $\|\mathcal{R}_\delta^{\text{pd}*} g\|_{L^2(\Omega)}^2 \leq 4\sqrt{2}\pi \frac{\delta_x}{\delta_s} \left\lceil \frac{\delta_s}{\delta_x} \right\rceil \|g\|_{L^2(\mathcal{S})}^2$ . If  $\frac{\delta_x}{\delta_s} \leq c$ , then  $\left\lceil \frac{\delta_s}{\delta_x} \right\rceil \leq (c+1) \frac{\delta_s}{\delta_x}$ , implying  $\|\mathcal{R}_\delta^{\text{pd}}\|^2 = \|\mathcal{R}_\delta^{\text{pd}*}\|^2 \leq 4\sqrt{2}\pi(c+1)$  for such  $\delta$ .

*Proof (Theorem 1).* The proofs of  $(\text{conv}^{\text{rd}})$ ,  $(\text{conv}^{\text{rd}*})$  and  $(\text{conv}^{\text{pd}*})$  will work as follows. First, we show convergence for smooth functions using Taylor's theorem and estimates from Lemmas 2 and 3. Once this is achieved, the convergence statements for general  $L^2$  functions is obtained using a diagonal argument that exploits the boundedness described in Lemma 4.

(conv<sup>rd</sup>): Let  $f \in \mathcal{C}_c^\infty(\Omega)$  (infinitely differentiable and compactly supported). We fix  $n \in \mathbb{N}$ , set  $\delta = \delta^n$  and all quantities relating to the discretization like  $X_{ij}$  or  $\mathcal{R}_\delta^{\text{rd}}$  are meant with regards to this specific  $\delta$ . Let  $(\phi, s) \in \mathcal{S}$  and let  $q \in [N_\phi]$  and  $p \in [N_s]$  be such that  $(\phi, s) \in \Phi_q \times S_p$ . Using the triangle inequality and Taylor's theorem, we have

$$\begin{aligned} |[\mathcal{R}f](\phi, s) - [\mathcal{R}f](\phi_q, s_p)| &\leq \int_{-1}^1 |f(s\vartheta_\phi + t\vartheta_\phi^\perp) - f(s_p\vartheta_q + t\vartheta_q^\perp)| dt \\ &\leq 2\|\nabla f\|_{L^\infty} \max_{t \in [-1, 1]} \|(s\vartheta_\phi + t\vartheta_\phi^\perp) - (s_p\vartheta_q + t\vartheta_q^\perp)\| \leq 4\|\nabla f\|_{L^\infty}(\delta_s + \delta_\phi), \end{aligned} \quad (16)$$

where we estimated the maximum term by  $\frac{\delta_s}{2} + 2\delta_\phi$  since  $s \in S_p$  and  $\phi \in \Phi_q$ . (Note that  $f$  being smooth,  $\mathcal{R}f$  is defined pointwise and not only almost everywhere.)

We set  $f_\delta = \sum_{i,j=0}^{N_x-1} f_{ij}u_{ij} \in U_\delta$  with  $f_{ij} = \frac{1}{\delta_x^2} \int_{X_{ij}} f(x) dx$  (the function  $f_\delta$  is again understood  $\mathcal{H}^1$  almost everywhere). Using Taylor's theorem,

$$|f(x) - f_\delta(x)| \leq \sqrt{2}\delta_x \|\nabla f\|_{L^\infty} \quad \text{for } \mathcal{H}^1 \text{ almost all } x \in \Omega \quad (17)$$

(the only exceptions are corners of pixels  $X_{ij}$ ). Thus, we have

$$\begin{aligned} |[\mathcal{R}f](\phi_q, s_p) - [\mathcal{R}_\delta^{\text{rd}}f](\phi, s)| &\stackrel{(\text{exact}^{\text{rd}})}{=} |[\mathcal{R}(f - f_\delta)](\phi_q, s_p)| \\ &\stackrel{(17)}{\leq} 2\sqrt{2}\delta_x \|\nabla f\|_{L^\infty}, \end{aligned} \quad (18)$$

where we used  $\|\mathcal{R}f\|_{L^\infty} \leq 2\|f\|_{L^\infty}$ . Combining (16) and (18), we see that

$$|[\mathcal{R}f - \mathcal{R}_\delta^{\text{rd}}f](\phi, s)| \leq 4(\delta_x + \delta_\phi + \delta_s)\|\nabla f\|_{L^\infty} \quad \text{for all } (\phi, s) \in \mathcal{S}, \quad (19)$$

implying  $\|\mathcal{R}f - \mathcal{R}_{\delta^n}^{\text{rd}}f\|_{L^2(\mathcal{S})} \rightarrow 0$  as  $n \rightarrow \infty$  (and  $\delta^n \rightarrow 0$ ).

Let  $f \in L^2(\Omega)$  not necessarily smooth or compactly supported, and let  $\epsilon > 0$ . There is an  $\tilde{f} \in \mathcal{C}_c^\infty(\Omega)$  such that  $\|f - \tilde{f}\|_{L^2(\Omega)} \leq \epsilon$  (since  $\mathcal{C}_c^\infty(\Omega)$  is dense in  $L^2(\Omega)$ ). There is an  $N = N(\epsilon, \tilde{f}) \in \mathbb{N}_0$  such that  $\|\mathcal{R}\tilde{f} - \mathcal{R}_{\delta^n}^{\text{rd}}\tilde{f}\|_{L^2(\mathcal{S})} \leq \epsilon$  for all  $n > N$  (as discussed in the previous paragraph). Then, for  $n > N$ , we have

$$\begin{aligned} \|\mathcal{R}f - \mathcal{R}_{\delta^n}^{\text{rd}}f\|_{L^2(\mathcal{S})} &\leq \|\mathcal{R}f - \mathcal{R}\tilde{f}\|_{L^2} + \|\mathcal{R}\tilde{f} - \mathcal{R}_{\delta^n}^{\text{rd}}\tilde{f}\|_{L^2} + \|\mathcal{R}_{\delta^n}^{\text{rd}}\tilde{f} - \mathcal{R}_{\delta^n}^{\text{rd}}f\|_{L^2} \\ &\leq (\|\mathcal{R}\| + \|\mathcal{R}_{\delta^n}^{\text{rd}}\|)\|f - \tilde{f}\|_{L^2} + \|\mathcal{R}\tilde{f} - \mathcal{R}_{\delta^n}^{\text{rd}}\tilde{f}\|_{L^2} \leq C\epsilon, \end{aligned} \quad (20)$$

where  $C = \|\mathcal{R}\| + \sup_n \{\|\mathcal{R}_{\delta^n}^{\text{rd}}\|\} + 1 < \infty$  using (BD<sup>rd</sup>) when  $\frac{\delta_s^n}{\delta_x^n} \leq c$  (as assumed). Thus, for any  $\epsilon > 0$ , we have  $\|\mathcal{R}f - \mathcal{R}_{\delta^n}^{\text{rd}}f\|_{L^2(\mathcal{S})} \leq C\epsilon$  for all  $n > M = M(\epsilon, f)$ , implying (conv<sup>rd</sup>).

(conv<sup>rd\*</sup>) & (conv<sup>pd\*</sup>): Let  $g \in \mathcal{C}_c^\infty(\mathcal{S})$ . Due to the compact support, we have  $g(\phi, s) = 0$  for all  $\phi$  and  $|s| > C$  with some constant  $0 < C < 1$ . Again, we fix  $n \in \mathbb{N}$  and all discretization quantities depend implicitly on  $\delta = \delta^n$ .

Given  $x \in \Omega$ , let  $i, j \in [N_x]$  be such that  $x \in X_{ij}$ . We reformulate the definition of  $\mathcal{R}^*$  and  $\mathcal{R}_\omega^*$  (in (2) and (7)) to see

$$\begin{aligned} [\mathcal{R}^* g - \mathcal{R}_\omega^* g](x) &= \sum_{q=0}^{N_\phi-1} \int_{\Phi_q} g(\phi, x \cdot \vartheta_\phi) \left( 1 - \delta_s \sum_{p=0}^{N_s-1} \mathbf{I}(ij, q, p) \right) \\ &\quad + \sum_{p=0}^{N_s-1} \mathbf{I}(ij, q, p) \mathbf{II}(x, \phi, p) \, d\phi \end{aligned} \quad (21)$$

with  $\mathbf{I}(ij, q, p) := \omega(\phi_q, x_{ij} \cdot \vartheta_q - s_p)$ ,  $\mathbf{II}(x, \phi, p) := \int_{S_p} g(\phi, x \cdot \vartheta_\phi) - g(\phi, s) \, ds$ .

The approach for showing both  $(\text{conv}^{\text{rd}*})$  and  $(\text{conv}^{\text{pd}*})$  is quite similar when considering (21) with  $\omega = \omega_{\delta_x}^{\text{rd}}$  or  $\omega = \omega_{\delta_s}^{\text{pd}}$ . We want  $\sum_{p=0}^{N_s-1} \mathbf{I}(ij, q, p) \approx \frac{1}{\delta_s}$ , and when  $\mathbf{I}(ij, q, p) \neq 0$ , we estimate  $\mathbf{II}(x, \phi, p)$  using Taylor's theorem. Thus, we will obtain pointwise convergence for this fixed smooth  $g$ . The conclusion for general  $g \in L^2(\mathcal{S})$  then follows via a diagonal argument analogous to (20).

$(\text{conv}^{\text{rd}*})$ : If  $|x_{ij} \cdot \vartheta_q| < 1 - \frac{\delta_x}{\sqrt{2}}$  for fixed  $q$ , we have  $\sum_{p=0}^{N_s-1} \mathbf{I}(ij, q, p) \in \frac{1}{\delta_s} + [-\frac{\sqrt{8}}{\delta_x}, \frac{\sqrt{8}}{\delta_x}]$  according to  $(\sum_p^{\text{rd}})$ . When  $|x_{ij} \cdot \vartheta_q| \geq 1 - \frac{\delta_x}{\sqrt{2}}$  on the other hand, we have  $g(\phi, x \cdot \vartheta_\phi) = 0$  since

$$|x \cdot \vartheta_\phi| \geq |x_{ij} \cdot \vartheta_q| - \frac{1}{\sqrt{2}} \delta_x - \delta_\phi \geq 1 - \sqrt{2} \delta_x - \delta_\phi > C \quad (22)$$

for  $\delta_x$  and  $\delta_\phi$  sufficiently small. In conclusion, the summand in the first row of (21) is bounded by  $\sqrt{8} \frac{\delta_x}{\delta_s} \|g\|_{L^\infty}$  if  $\delta$  is sufficiently small.

In order to estimate  $\mathbf{II}$ , we estimate the difference in arguments of  $g$  in  $\mathbf{II}$  by

$$\begin{aligned} |x \cdot \vartheta_\phi - s| &\leq \|x - x_{ij}\| + |x_{ij} \cdot \vartheta_\phi - x_{ij} \cdot \vartheta_q| + |x_{ij} \cdot \vartheta_q - s_p| + |s_p - s| \\ &\leq \frac{1}{2} \delta_s + \sqrt{2} \delta_x + \delta_\phi \leq \frac{3}{2} (\delta_x + \delta_s + \delta_\phi) \end{aligned} \quad (23)$$

if  $\phi \in \Phi_q$ ,  $s \in S_p$  and  $\mathbf{I}(ij, q, p) \neq 0$  (i.e.,  $|x_{ij} \cdot \vartheta_q - s_p| < \frac{\delta_x}{\sqrt{2}}$ ). We use Taylor's theorem to estimate that if  $\mathbf{I}(ij, q, p) \neq 0$  and  $x \in X_{ij}$ , then

$$|\mathbf{II}(x, \phi, p)| \leq \frac{3}{2} \delta_s (\delta_x + \delta_s + \delta_\phi) \|\nabla g\|_{L^\infty} + o(\delta) \delta_s. \quad (24)$$

Moreover, we have  $\sum_{p=0}^{N_s-1} |\mathbf{I}(ij, q, p)| \leq \frac{1}{\delta_s} + \frac{\sqrt{8}}{\delta_x}$  in any case; see  $(\sum_p^{\text{rd}})$ . So the second line of (21) can be estimated by  $\frac{3}{2} (1 + \sqrt{8} \frac{\delta_x}{\delta_s}) (\delta_x + \delta_s + \delta_\phi) \|\nabla g\|_{L^\infty} + o(\delta)$ . Finally, note that  $\sum_{q=0}^{N_\phi-1} \int_{\Phi_q} 1 \, d\phi = \pi$ . In conclusion, using (21), we have

$$\left| [\mathcal{R}^* g - \mathcal{R}_\delta^{\text{rd}*} g](x) \right| \leq \sqrt{8} \pi \frac{\delta_s}{\delta_x} \|g\|_{L^\infty} + \frac{3}{2} \pi \left( 1 + \sqrt{8} \frac{\delta_s}{\delta_x} \right) (\delta_x + \delta_s + \delta_\phi) \|\nabla g\|_{L^\infty} + o(\delta) \quad (25)$$

if  $\delta$  is sufficiently small. When increasing  $n \rightarrow \infty$  (and thus  $\delta^n \rightarrow 0$ ), we therefore obtained the desired convergence  $\|\mathcal{R}^* g - \mathcal{R}_{\delta^n}^{\text{rd}^*} g\|_{L^2(\mathcal{S})} \rightarrow 0$  for smooth functions  $g$  (assuming  $\frac{\delta_s^n}{\delta_x^n} \xrightarrow{n \rightarrow \infty} 0$ ). The convergence for general  $g \in L^2(\mathcal{S})$  follows using a diagonal argument analogous to (20) (with  $\|\mathcal{R}_{\delta}^{\text{rd}^*}\|$  bounded due to  $(\text{BD}^{\text{rd}})$ ).

( $\text{conv}^{\text{pd}^*}$ ): For  $|x_{ij} \cdot \vartheta_q| < 1 - \frac{\delta_s}{2}$  ( $= |s_0| = |s_{N_s-1}|$ ), we have  $\sum_{p=0}^{N_s-1} \text{I}(ij, q, p) = \frac{1}{\delta_s}$  via  $(\text{intpol}^{\text{pd}})$ . Again, if  $|x_{ij} \cdot \vartheta_q| \geq 1 - \frac{\delta_s}{2}$ , the corresponding  $g(\phi, x \cdot \vartheta_\phi)$  (with  $x \in X_{ij}$  and  $\phi \in \Phi_q$ ) equals 0 for  $\delta$  sufficiently small since

$$|x \cdot \vartheta_\phi| > |x_{ij} \cdot \vartheta_q| - \frac{\delta_x}{\sqrt{2}} - \delta_\phi > 1 - \frac{\delta_s}{2} - \frac{\delta_x}{\sqrt{2}} - \delta_\phi > C. \quad (26)$$

Hence, the summand in the first row of (21) is zero.

Again,  $|\text{II}(x, \phi, p)| \leq \frac{3}{2} \delta_s (\delta_s + \delta_x + \delta_\phi) \|\nabla g\|_{L^\infty} + o(\delta)$  if  $\text{I}(ij, q, p) \neq 0$  (with  $x \in X_{ij}$  and  $\phi \in \Phi_q$ ) using Taylor's theorem. Moreover,  $\sum_{p=0}^{N_s-1} |\text{I}(ij, q, p)| \leq \frac{1}{\delta_s}$ .

In conclusion, we have

$$|[\mathcal{R}^* g - \mathcal{R}_{\delta}^{\text{pd}^*} g](x)| \leq \pi (\delta_s + \delta_x + \delta_\phi) \frac{3}{2} \|\nabla g\|_{L^\infty} + o(\delta) \quad (27)$$

for all  $x \in \Omega$  if  $\delta$  is sufficiently small, implying  $\|\mathcal{R}^* g - \mathcal{R}_{\delta^n}^{\text{pd}^*} g\|_{L^2(\Omega)} \rightarrow 0$  as  $n \rightarrow \infty$ . The proof for general  $g \in L^2(\mathcal{S})$  follows again by a diagonal argument analogous to (20) (using  $(\text{BD}^{\text{pd}})$ ).

## 4 Numerical Experiments

## 5 Conclusion and Outlook

This paper presented a novel interpretation of the ray-driven and pixel-driven discretization frameworks as convolutional discretizations. We prove convergence statements in the strong operator topology (i.e., pointwise) for these methods in Theorem 1. This result gives a theoretical foundation to the widespread use of ray-driven forward and pixel-driven backprojection operators under balanced resolutions, confirming anecdotal reports concerning approximation properties. Our result claims nothing concerning the convergence for the ray-driven backprojection and pixel-driven Radon transform under balanced resolutions, though anecdotes suggest these do not converge; or at least significantly slower. Hence, the combination of ray-driven and pixel-driven methods ( $\text{rd-pd}^*$ ) is perhaps the best one can do while maintaining the balanced resolution setting.

These results are probably extendable in a straightforward manner to other types of tomography like fanbeam or conebeam operators, and this might be the topic of future investigations.

Note that this work did not address the issue of unmatched operators. However, if the alternative is using non-approximating operators, unmatched operators are perhaps preferable.



The convergence result ( $\text{conv}^{\text{rd}*}$ ) shows that while the ray-driven backprojection might be unsuitable for balanced resolutions, it indeed approximates the backprojection if  $\frac{\delta_s}{\delta_x} \rightarrow 0$ . Thus, future work might investigate if convergence in the operator norm is achieved in that setting.

**Acknowledgement.** This work was supported by The Villum Foundation (Grant No.25893) and is in part based on work supported by the International Research Training Group “Optimization and Numerical Analysis for Partial Differential Equations with Nonsmooth Structures”, funded by the German Research Council (DFG) and Austrian Science Fund (FWF) grant W1244.

## References

1. Andersen, A.H., Kak, A.C.: Simultaneous algebraic reconstruction technique (SART): A superior implementation of the ART algorithm. *Ultrasonic Imaging* **6**(1), 81–94 (1984)
2. Bredies, K., Huber, R.: Convergence analysis of pixel-driven Radon and fan-beam transforms. *SIAM Journal on Numerical Analysis* **59**(3), 1399–1432 (2021). <https://doi.org/10.1137/20M1326635>
3. Deans, S.R.: *The Radon Transform and Some of Its Applications*. Krieger Publishing Company (1993)
4. Dong, B., Li, J., Shen, Z.: X-ray CT image reconstruction via wavelet frame based regularization and Radon domain inpainting. *Journal of Scientific Computing* **54**(2), 333–349 (2013). <https://doi.org/10.1007/s10915-012-9579-6>
5. Dong, Y., Hansen, P., Hochstenbach, M., Brogaard Riis, N.: Fixing nonconvergence of algebraic iterative reconstruction with an unmatched backprojector. *SIAM Journal on Scientific Computing* **41**(3), A1822–A1839 (2019)
6. Gao, H.: Fast parallel algorithms for the X-ray transform and its adjoint. *Medical Physics* **39**(11), 7110–7120 (2012). <https://doi.org/10.1118/1.4761867>
7. Gilbert, P.: Iterative methods for the three-dimensional reconstruction of an object from projections. *Journal of Theoretical Biology* **36**(1), 105–117 (1972)
8. Hsieh, J.: *Computed Tomography: Principles, Design, Artifacts, and Recent Advances*. WA: SPIE — The International Society for Optical Engineering (2009)
9. Huber, R.: Pixel-driven projection methods’ approximation properties and applications in electron tomography. PhD thesis, University of Graz, Austria (2022)
10. Huber, R.: A novel interpretation of the Radon transform’s ray- and pixel-driven discretizations under balanced resolutions. Accepted to the SSVM 2025 (Scale Space and Variational Methods in Computer Vision) (2025)
11. Huber, R., Haberfehlner, G., Holler, M., Kothleitner, G., Bredies, K.: Total generalized variation regularization for multi-modal electron tomography. *Nanoscale* **11**, 5617–5632 (2019). <https://doi.org/10.1039/C8NR09058K>
12. Liu, R., Fu, L., De Man, B., Yu, H.: Gpu-based branchless distance-driven projection and backprojection. *IEEE Transactions on Computational Imaging* **3**(4), 617–632 (2017). <https://doi.org/10.1109/TCI.2017.2675705>
13. Lorenz, D., Schneppe, F.: Chambolle–pock’s primal-dual method with mismatched adjoint. *Applied Mathematics & Optimization* **87**(2) (2023). <https://doi.org/10.1007/s00245-022-09933-5>

14. Natterer, F.: The Mathematics of Computerized Tomography. Society for Industrial and Applied Mathematics, Philadelphia (2001)
15. Peters, T.M.: Algorithms for fast back- and re-projection in computed tomography. IEEE Transactions on Nuclear Science **28**(4), 3641–3647 (1981). <https://doi.org/10.1109/TNS.1981.4331812>
16. Qiao, Z., Redler, G., Gui, Z., Qian, Y., Epel, B., Halpern, H.: Three novel accurate pixel-driven projection methods for 2D CT and 3D EPR imaging. Journal of X-ray science and technology **26**(1), 83–102 (2017)
17. Scales, J.: Tomographic inversion via the conjugate gradient method. Geophysics **52**, 179–185 (1987). <https://doi.org/10.1190/1.1442293>
18. Scherzer, O., Grasmair, M., Grossauer, H., Haltmeier, M., Lenzen, F.: Variational Methods in Imaging. Springer, 1 edn. (2008)
19. Siddon, R.L.: Fast calculation of the exact radiological path for a three-dimensional CT array. Medical Physics **12**(2), 252–255 (1985)
20. Sundermann, E., Jacobs, F., Christiaens, M., De Sutter, B., Lemahieu, I.: A fast algorithm to calculate the exact radiological path through a pixel or voxel space. Journal of Computing and Information Technology **6**, 89–94 (1998)
21. Zhuang, W., Gopal, S.S., Hebert, T.J.: Numerical evaluation of methods for computing tomographic projections. IEEE Transactions on Nuclear Science **41**(4), 1660–1665 (1994). <https://doi.org/10.1109/23.322963>

## A Appendix: Proof of Lemma 1

We fix some  $\phi \in [0, \pi[$  and  $s \in \mathbb{R}$ , and set  $\underline{s} = \underline{s}(\phi)$  and  $\bar{s} = \bar{s}(\phi)$  for the sake of readability. Recall that  $|s|$  describes the normal distance of  $L_{\phi,s}$  to the origin  $(0, 0) \in \mathbb{R}^2$ , and a point  $x$  satisfies  $x \in L_{\phi,s}$  if and only if  $x \cdot \vartheta_\phi = s$ . In particular, all points  $x$  with  $x \cdot \vartheta_\phi > s$  are on one side of  $L_{\phi,s}$ , and all  $x$  with  $x \cdot \vartheta_\phi < s$  on the other.

We consider the square  $Z := [-\frac{\delta_x}{2}, \frac{\delta_x}{2}]^2$ . Our first goal is to show

$$\delta_x^2 \omega_{\delta_x}^{\text{rd}}(\phi, s) = \mathcal{H}^1(L_{\phi,s} \cap Z) - \frac{1}{2} \mathcal{H}^1(L_{\phi,s} \cap \partial Z) =: F(\phi, s), \quad (28)$$

from which (5) will easily follow.

We divide the calculation of (28) into multiple cases. Since the following considerations are quite geometric, see Figure 5 for their visual representation. Via straightforward calculation, the four corners  $(\pm \frac{\delta_x}{2}, \pm \frac{\delta_x}{2}) \in \mathbb{R}^2$  of  $Z$  lie exactly on the lines associated with  $-\bar{s}$ ,  $-\underline{s}$ ,  $\underline{s}$  and  $\bar{s}$ . Therefore, if  $|s| < \underline{s}$  (case 1), i.e.,  $-\bar{s} \leq -\underline{s} < s < \underline{s} \leq \bar{s}$ , there are two vertices on either side of  $L_{\phi,s}$ . If  $|s| \in [\underline{s}, \bar{s}[$  (case 2), then one side of  $L_{\phi,s}$  has only a single corner. If  $|s| > \bar{s}$  (case 3), then one side of  $L_{\phi,s}$  does not contain any corners. This leaves the special cases  $|s| = \underline{s}$  and  $\phi \notin \frac{\pi}{2}\mathbb{Z}$  (case 4),  $|s| = \bar{s}$  and  $\phi \notin \frac{\pi}{2}\mathbb{Z}$  (case 5), and finally  $|s| = \bar{s}$  and  $\phi \in \frac{\pi}{2}\mathbb{Z}$  implying  $\underline{s} = \bar{s}$  (case 6).

Moreover, note that  $L_{\phi,s} \cap \partial Z$  contains exactly two points when  $|s| < \bar{s}$  and thus is an  $\mathcal{H}^1$  null set. When  $|s| = \bar{s}$ , there is exactly one element in  $L_{\phi,s} \cap \partial Z$  if  $\phi \notin \frac{\pi}{2}\mathbb{Z}$  (i.e.,  $L_{\phi,s}$  is not parallel to one of the sides of  $Z$ ), and it is one entire side of  $Z$  otherwise. Hence,  $\mathcal{H}^1(L_{\phi,s} \cap \partial Z)$  is only non-zero in the case 6, and can otherwise be ignored.

Case 1: If  $|s| < \underline{s}$ , we consider the right triangle formed by the two points  $z_1, z_2 \in L_{\phi, s} \cap \partial Z$  (lying on opposite sides of  $Z$ ) and one point exactly opposite  $z_1$ ; see Figure 5 b). Hence, one side of the triangle is  $L_{\phi, s} \cap Z$  with length  $r$ , and one other side's length is  $\delta_x$ . Since one of the triangle's sides is  $\delta_x$  long and it contains the angle  $\phi$ , the hypotenuse's length equals  $F(\phi, s) = r = \delta_x \min\left(\frac{1}{|\cos(\phi)|}, \frac{1}{|\sin(\phi)|}\right) \stackrel{\text{per}}{\stackrel{\text{def}}{=} } \delta_x^2 \omega_{\delta_x}^{\text{rd}}(\phi, s)$ .

Case 2: When  $|s| \in [\underline{s}, \bar{s}]$ , the two points of  $L_{\phi, s} \cap \partial Z$  form a right triangle with the single corners of  $Z$  on one side of  $L_{\phi, s}$ . In particular,  $L_{\phi, s} \cap Z$  forms the hypotenuse of said triangle with length  $r$ , while we denote the catheti's lengths by  $a$  and  $b$ , and the height as  $h$ ; see Figure 5 c). We note that the height satisfies  $h = \bar{s} - |s|$ . The area in a right triangle satisfies  $\text{Area} = \frac{ab}{2} = \frac{rh}{2}$ , which together with  $a = r|\sin(\phi)|$  and  $b = r|\cos(\phi)|$  implies

$$F(\phi, s) = r = \frac{h}{|\cos(\phi)\sin(\phi)|} = \frac{\bar{s} - |s|}{|\cos(\phi)\sin(\phi)|} \stackrel{\text{per}}{\stackrel{\text{def}}{=} } \delta_x^2 \omega_{\delta_x}^{\text{rd}}(\phi, s). \quad (29)$$

Case 3: Since  $Z$  is the convex hull of its corners,  $Z$  in its entirety lies on one side of  $L_{\phi, s}$  if  $|s| > \bar{s}$ , and thus  $L_{\phi, s} \cap Z = \emptyset$ , implying  $F(\phi, s) = 0 \stackrel{\text{per}}{\stackrel{\text{def}}{=} } \delta_x^2 \omega_{\delta_x}^{\text{rd}}(\phi, s)$ .

Case 4: Since  $\phi \notin \frac{\pi}{2}\mathbb{Z}$  (implying  $\underline{s} < \bar{s}$ ),  $|s| = \underline{s}$  is precisely the same situation as described in case 2.

Case 5: In the case  $\phi \notin \frac{\pi}{2}\mathbb{Z}$  and  $|s| = \bar{s}$ , the intersection  $L_{\phi, s} \cap Z$  contains only a single point (the corner), thus having Hausdorff measure zero, which coincides with  $\delta_x^2 \omega_{\delta_x}^{\text{rd}}(\phi, s)$  (this falls into the 'else' case of (3)).

Case 6: If  $\phi \in \frac{\pi}{2}\mathbb{Z}$  and  $|s| = \bar{s}$ , we have to take  $\partial Z$  into account (this is the only case where the Hausdorff measure of  $L_{\phi, s} \cap \partial Z$  is not zero). In particular,  $L_{\phi, s} \cap Z = L_{\phi, s} \cap \partial Z$  is one side of  $Z$ , and thus  $\mathcal{H}^1(L_{\phi, s} \cap Z) = \mathcal{H}^1(L_{\phi, s} \cap \partial Z) = \delta_x$ . Therefore,  $F(\phi, s) = \delta_x - \frac{\delta_x}{2} = \frac{\delta_x}{2} \stackrel{\text{per}}{\stackrel{\text{def}}{=} } \delta_x^2 \omega_{\delta_x}^{\text{rd}}(\phi, s)$ .

In conclusion, (28) holds. Since the Hausdorff measure is translation invariant,  $X_{ij} = x_{ij} + Z$  and  $L_{\phi, s} = x_{ij} + L_{\phi, s-x_{ij}\cdot\vartheta_\phi}$ , we finally get

$$\mathcal{H}^1(L_{\phi, s} \cap X_{ij}) = \mathcal{H}^1((x_{ij} + L_{\phi, s-x_{ij}\cdot\vartheta_\phi}) \cap (x_{ij} + Z)) = \mathcal{H}^1(L_{\phi, s-x_{ij}\cdot\vartheta_\phi} \cap Z). \quad (30)$$

and analogously for  $\mathcal{H}^1(L_{\phi, s} \cap \partial X_{ij})$ , resulting in (5).

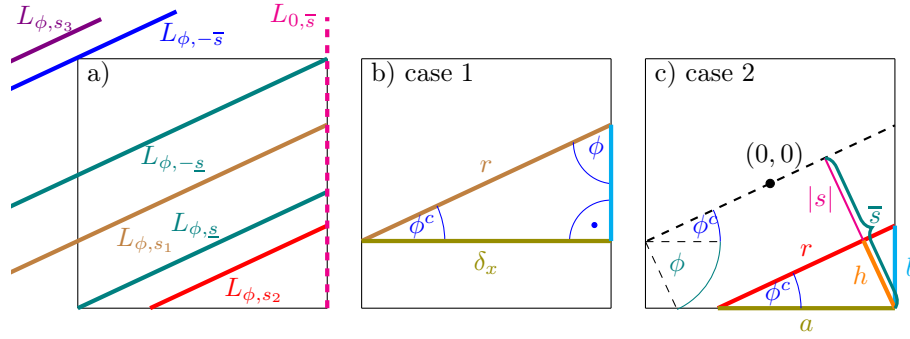


**Fig. 5.** Illustration supporting the proof of Lemma 1. In a), we depict the different cases passing through a square  $Z$  for fixed  $\phi$  (here  $105^\circ$ ), where the teal lines describe the case 4  $|s| = \underline{s}(\phi)$  in which the corners are precisely hit, the brown line  $|s_1| < \underline{s}(\phi)$  (case 1) and the red line  $|s_2| \in [\underline{s}(\phi), \bar{s}(\phi)[$  (case 2). Moreover, the blue line is representative of case 5 (hitting exactly one corner), while the violet line representing case 3 does not hit  $Z$ , and the dashed magenta line is representative of case 6 with the line intersecting with one side of  $Z$ . Figures b) and c) detail the geometry of case 1 and case 2, depicting relevant right triangles.